Journal of the Korean Ceramic Society
Vol. 41, No. 1, pp. 1~8, 2004.

Mechanical Behavior of Directionally Solidified $(Y_2O_3)ZrO_2/Al_2O_3$ Eutectic Fibers

Deok-Yong Park† and Jenn-Ming Yang*

Department of Applied Materials Engineering, Hanbat National University, Daejeon 305-719, Korea
**Department of Materials Science and Engineering, University of California, Los Angeles, CA 90095, U.S.A.*
(Received September 18, 2003; Accepted December 6, 2003)

ABSTRACT

The microstructural features and mechanical behavior of directionally solidified $(Y_2O_3)ZrO_2/Al_2O_3$ eutectic fibers after extended heat treatment in oxidizing environment were investigated. The fiber was grown continuously by an Edge-defined Film-fed Growth (EFG) technique. The microstructure was characterized using X-Ray Diffraction (XRD) and Scanning Electron Microscopy (SEM). The microstructure of the fiber in the as-fabricated state consists of highly oriented colony and fine lamellar microstructure along the fiber axis. Tensile strength of the $(Y_2O_3)ZrO_2/Al_2O_3$ eutectic fiber remained unchanged with heat treatment at temperatures between 1200°C and 1500°C up to 300 h. The Weibulls modulus remained fairly constant after extended thermal exposure. The fracture toughness and crack propagation behavior were investigated. The fracture toughness (K_{1C}) of the $(Y_2O_3)ZrO_2/Al_2O_3$ eutectic fiber in the as-fabricated state were measured to be 3.6 ± 0.5 MPa·m$^{1/2}$ by an indentation technique and 2.2 ± 0.2 MPa·m$^{1/2}$ by assuming elliptical flaw of a semi-infinite solid, respectively. The $(Y_2O_3)ZrO_2/Al_2O_3$ eutectic fiber showed a radial (Palmqvist) crack type and exhibited an orthotropic crack growth behavior under 100 g load.

Key words : Directional solidification, In-situ composites, Ceramic fiber, Mechanical properties

1. Introduction

Oxide-based fibers are the most promising materials as the reinforcing materials for high temperature structural applications in oxidizing environments because of their inherent thermal stability. As a result, several single-crystal oxide fibers (such as Al_2O_3, $MgAl_2O_4$, $Y_3Al_5O_{12}$, ZrO_2, and Y_2O_3-stabilized ZrO_2)[1-7] and oxide-oxide eutectic fibers (such as $Y_3Al_5O_{12}/Al_2O_3$, $Al_2O_3/ZrO_2(Y_2O_3)$, CeO_2-doped $Y_3Al_5O_{12}/Al_2O_3$, and Pr_2O_3-doped $Y_3Al_5O_{12}/Al_2O_3$) have been developed.[8-14] Among the single crystal oxides and oxide-oxide eutectics, the directionally solidified $Y_3Al_5O_{12}/Al_2O_3$ eutectic system has been demonstrated as one of the most promising systems because of its chemical, microstructural, mechanical, and thermal stability.[15,16] Even though the directionally solidified $Y_3Al_5O_{12}/Al_2O_3$ eutectic fiber proved to be a promising material for high temperature structural applications in oxidizing environments, there is still a need for a fiber with a higher coefficient of thermal expansion to use in intermetallic and metal matrix composites.

Recently, the Al_2O_3-ZrO_2 system has also received considerable attention as a high temperature structural material due to its high strength and high toughness. It was reported that the alumina/zirconia (Al_2O_3/ZrO_2) eutectic fiber has a higher expansion coefficient than either alumina or YAG/alumina ($Y_3Al_5O_{12}/Al_2O_3$).[11] The eutectic temperature between alumina and zirconia is located at 38 mol% ZrO_2 (42.5 wt%) and 1910 ± 20°C.[17,18] Furthermore, it has been demonstrated that the $Al_2O_3/ZrO_2(Y_2O_3)$ eutectic retained its room-temperature strength at temperatures as high as 1575°C.[19] A previous study by Hulse and Batt also indicated that $Al_2O_3/ZrO_2(Y_2O_3)$ eutectic exhibits a higher fracture toughness than either polycrystalline or single-crystal Al_2O_3, especially at high temperatures.[19] The $Al_2O_3/ZrO_2(Y_2O_3)$ eutectic fiber has been successfully fabricated by both EFG and LHFZ (Laser Heated Floating Zone) techniques.[13,20]

The fracture toughness is an important parameter to evaluate the mechanical performance of structural materials. Various different techniques are available for the measurement of the fracture toughness.[21-25] Indentation technique is one of the methods. Evans and Wilshaw suggested the indentation technique as a simple, easy and economic method to evaluate fracture toughness in a study of indentation fracture for ceramic materials.[26] Since Hertz first investigated the cone-shaped fracture at elastic contacts between glass lenses in 1896, indentation mechanics has become extensively used in the analysis and characterization of fracture and deformation properties of brittle ceramics, as well as metals and other materials.[27,28] Traditionally, Hertzian cone crack has been most widely studied in flat silicate glass plate, using sphere indenter of hardened steel or tungsten carbide. Extensive studies to other brittle solids such as single crystals and hard, fine-grain polycrystalline

†Corresponding author : Deok-Yong Park
E-mail : dypark@hanbat.ac.kr
Tel : +82-42-821-1278 Fax : +82-42-821-1592

ceramics become more prevalent in 1950s-1970s.[28] More recently, indentation tests with sharp indenters such as Vickers and Knoop indenters were developed in 1970s due to the geometrical similarity of the residual impressions; the contact pressure is independent of indent size, and thus affords a convenient measure of hardness.[29] Radial-median crack produced by diamond pyramid indenter is now the most widely used of all fracture testing methodologies in the mechanical evaluation of brittle materials.

The purpose of this work is to study the microstructural stability and mechanical behavior of the directionally solidified $(Y_2O_3)ZrO_2/Al_2O_3$ eutectic fibers after extended thermal exposure in an oxidizing environment.

2. Experimental Procedure

$(Y_2O_3)ZrO_2/Al_2O_3$ eutectic fiber produced by Saphikon Inc. (Milford, NH, USA) with a nominal diameter of 125 μm were used in this study. The fibers were grown continuously by an EFG technique with a grown rate of 2.03 cm/min. The composition of the $(Y_2O_3)ZrO_2/Al_2O_3$ eutectic fiber was slightly hypereutectic; 60.8 mol% Al_2O_3 and 39.2 mol% ZrO_2 (including 9.5 mol% Y_2O_3). In the EFG process, a refractory metal die is partially immersed in a crucible containing the melt with the above composition. Liquid from the melt rises in capillaries in the die and wets upper surface of the die. A seed crystal is touched to the liquid film on the die surface and withdrawn. As it is withdrawn, the crystal grows continuously downward toward the liquid film from which it is being pulled. A detailed description of the EFG process can be found elsewhere.[30,31] X-ray diffractometer (Model 42202, Norelco, North American Phillips Company Inc.) with CuK_α radiation was used for the identification of the phases in the $(Y_2O_3)ZrO_2/Al_2O_3$ eutectic fiber. Microstructures of the $(Y_2O_3)ZrO_2/Al_2O_3$ eutectic fiber at the interior section along the growth direction (the longitudinal section along the fiber axis) and the cross-sectional areas were examined using a scanning electron microscope (Stereoscan 250, Cambridge, Scientific Instruments Ltd., Valencia, CA, USA). The backscattered electron image was used to identify the microstructure of the $(Y_2O_3)ZrO_2/Al_2O_3$ eutectic fiber at the longitudinal and the cross-sectional areas. Tensile test were conducted at room temperature using an Instron universal testing machine (Model 5544, Instron Corp., Canton, MA, USA) with a crosshead speed of 0.127 mm/min. Fibers ends were mounted on end tabs with epoxy for gripping. A gage length of 2.54 cm was used. Prior to heat treatment and tensile testing, all the fibers were ultrasonically cleaned. To study the stability of the eutectic microstructure at high temperatures and its effect on tensile strength, the as-fabricated fibers were heat-treated at temperature between 1200°C and 1500°C in air for the duration of up to 300 h. A minimum of 30 fibers was tested so that the Weibulls cumulative distribution could be obtained.

Two different methods were used to evaluate the fracture toughness of the $(Y_2O_3)ZrO_2/Al_2O_3$ eutectic fiber. First, the fracture toughness of the fibers was calculated by assuming an elliptical flaw of a semi-infinite solid from the fractographic observation of the porosity after tensile test.[15]

$$K_{IC} = \frac{\sigma\sqrt{\pi a}}{\left(\frac{3\pi}{8} + \frac{\pi a^2}{8c^2}\right)} \tag{1}$$

where σ is the tensile strength, a and c are the depth and half width of the flaw, respectively. Second, an indentation technique was also conducted on the polished surface of the fiber to compare the fracture toughness (K_{IC}), using the following equations.[32]

$$K_{IC} = \beta \cdot (H_V W)^{1/2} \tag{2}$$

$$\beta = \frac{1}{3(1-\upsilon^2)(2^{1/2} \cdot \pi \cdot \tan\Psi)^{1/3}} \tag{3}$$

where β is a non-dimensional constant dependent on the indenter geometry ($\beta = 0.09698$), H_V is the hardness, W is a constant which is termed Palmqvist crack resistance, ν is the Poissons ratio ($\nu = 0.24$ provided and measured by Saphikon Inc.), and 2Ψ is the apex angle of the Vickers indenter (136° for the standard Vickers indenter). In this study, the longitudinal section of the fibers to the growth direction was polished to 0.1 μm diamond compounds finish. Vickers hardness tester (Micromet II Microhardness Tester, Buhler Ltd., Lake Bluff, Illinois, USA) was used to introduce a crack on the polished surface of the fiber. The cracks were generated under a load of 100 g (1 N load) and the crack lengths were measured using a SEM. Vickers hardness (H_v) and fracture toughness (K_{IC}) were determined by the average value of 20 readings.

3. Results and Discussion

3.1. Microstructural Stability and Tensile Behavior

The backscattered electron image of the longitudinal and cross section areas of $(Y_2O_3)ZrO_2/Al_2O_3$ eutectic fiber in the as-fabricated state are shown in Fig. 1. It was observed that the microstructure of the fiber in the as-fabricated state consists of elongated colony and fine lamellar microstructure along the fiber axis. The formation of colony structure in the eutectics has been shown to be associated with the presence of a cellular structure superimposed on the lamellar eutectic structure.[33] The fine lamellar structure with ZrO_2 (bright) and Al_2O_3 (dark) phases distributed uniformly within the colonies (Fig. 1(b) and (d)). At the colony boundaries, the morphology of ZrO_2 phase changes from lamellar to coarse discrete particles with irregular shape. Also, within each colony, those lamellae at the center were well-aligned, highly oriented, with high aspect ratio and parallel to the growth direction. However, outer lamellae curved toward the boundary as shown in Fig. 1(b). X-ray diffraction analysis of the $(Y_2O_3)ZrO_2/Al_2O_3$ eutectic fiber in the as-fabricated state indicated that it contained Al_2O_3 and ZrO_2 phases as shown in Fig. 2. Some $Y_3Al_5O_{12}$ peaks were

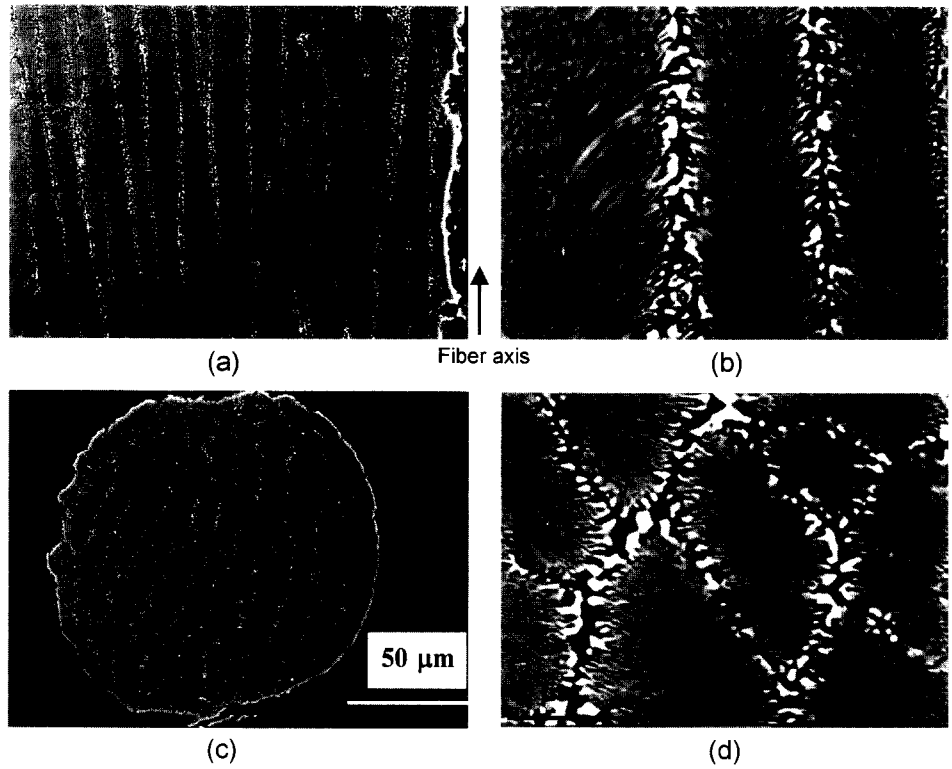

Fig. 1. Microstructures of $(Y_2O_3)ZrO_2/Al_2O_3$ eutectic fiber in the as-fabricated state (a) the longitudinal section area, low magnification, (b) the longitudinal section area, high magnification, (c) the cross section area, low magnification, and (d) the cross section area, high magnification.

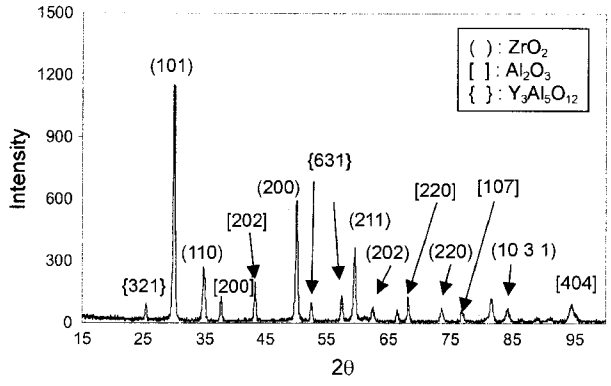

Fig. 2. XRD patterns of the $(Y_2O_3)ZrO_2/Al_2O_3$ eutectic fibers in the as-fabricated state.

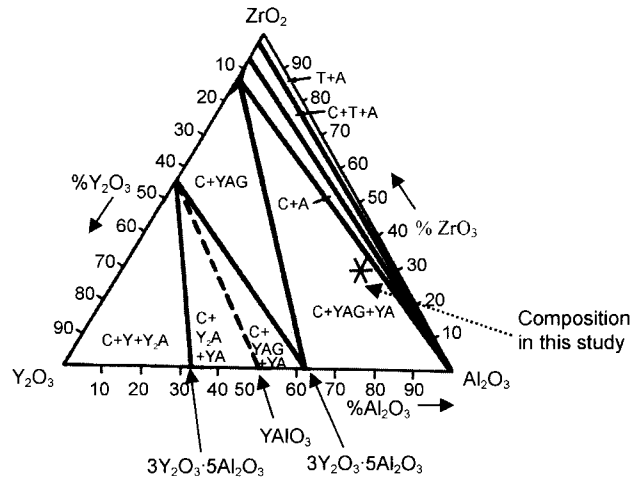

Fig. 3. Phase diagram of ZrO_2-Y_2O_3-Al_2O_3 system (C: cubic ZrO_2 solid solution, Y: Y_2O_3, A: Al_2O_3, YAG: $Y_3Al_5O_{12}$, T: tetragonal ZrO_2).[18]

detected in X-ray diffraction analysis. From the ternary phase diagram as shown in Fig. 3,[18] it is believed that the $Y_3Al_5O_{12}$ phase can exist in the $(Y_2O_3)ZrO_2/Al_2O_3$ eutectic fiber with the composition of 60.8 mol% Al_2O_3-39.2 mol% ZrO_2 (including 9.5 mol% Y_2O_3).

The tensile strength of the directionally solidified $(Y_2O_3)ZrO_2/Al_2O_3$ eutectic fiber before and after heat treatment at temperatures between 1200°C to 1500°C up to 300 h are shown in Fig. 4. The average tensile strength of the as-fabricated fibers at room temperature is 1.2 GPa. The tensile strength of the directionally solidified $(Y_2O_3)ZrO_2/Al_2O_3$ eutectic fiber grown by the EFG technique is similar to that of the LHFZ processed fiber.[11] The tensile strength remained fairly constant after annealing at temperatures between 1200°C and 1500°C up to 300 h. After heat treatment at high temperatures, the microstructural characteristics remained similar as shown in Fig. 5. However, the coarsening of the eutectic structure of the directionally solidified $(Y_2O_3)ZrO_2/Al_2O_3$ eutectic fiber was clearly observed. The thickness of ZrO_2 layer in the as-fabricated state was measured to be 0.08 μm. It increased to 0.36 and 0.58 μm after being heat-treated at 1300°C for 100 h and

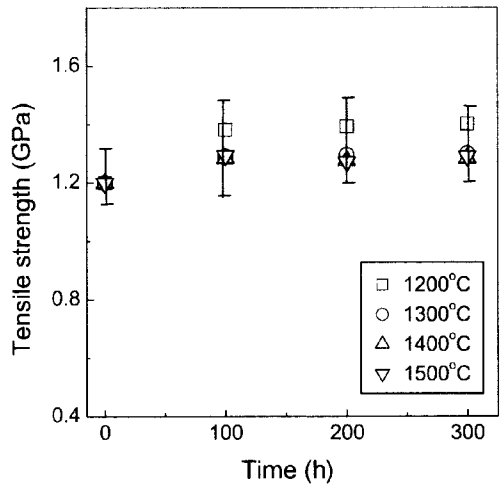

Fig. 4. The changes of tensile strength as a function of heat treatment time.

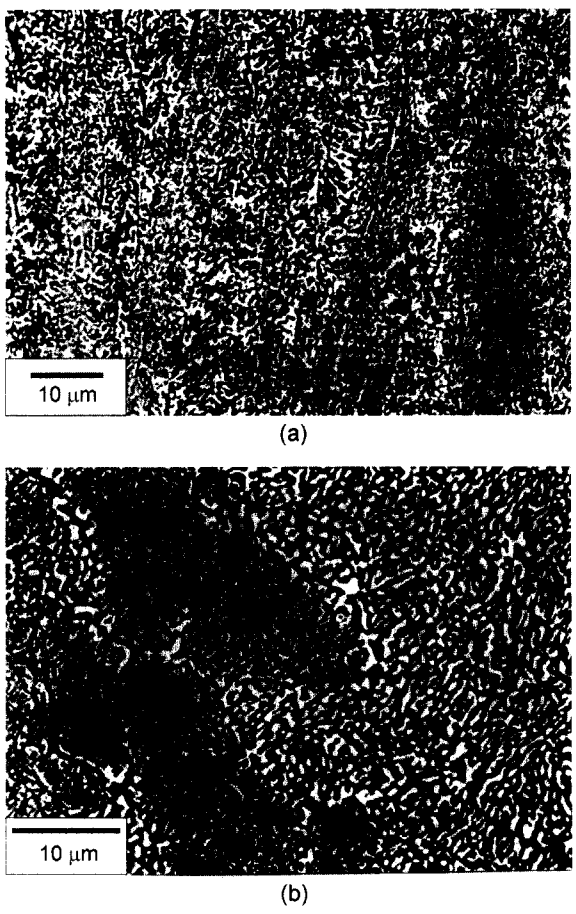

Fig. 5. Microstructures of $(Y_2O_3)ZrO_2/Al_2O_3$ eutectic fiber after heat treatment at 1500°C for 100 hours (a) the longitudinal section area, and (b) the cross section area.

1500°C for 100 h, respectively. Even though the thickness of both ZrO_2 and Al_2O_3 layers within the colony increased substantially, the thickness ratio of ZrO_2 and Al_2O_3 layers remained nearly constant (~1) after annealing at various temperatures and durations. It is evident that the changes of thickness of the ZrO_2 and Al_2O_3 layers after heat treatment did not affect on the room-temperature tensile strength. Courtright et al. also reported that annealing of the $(Y_2O_3)ZrO_2/Al_2O_3$ eutectic fiber grown by LHFZ process did not significantly affect on the tensile strengths.[12] The exact mechanisms leading to the excellent strength retention after annealing at elevated temperature have not yet been identified. However, Kennard *et al.*[34] reported that the tensile strength of the ZrO_2/MgO eutectic increased after heat treatment at 1200°C for 24 h because of a compressive stress in the ZrO_2 matrix resulting from the increase in volume during the cubic-to-monoclinic transformation. Therefore, the excellent strength retention after heat treatment in the $(Y_2O_3)ZrO_2/Al_2O_3$ eutectic fiber may be attributed to the phase transformation during annealing.

The distribution of fracture stresses of brittle materials, e.g. ceramics, is commonly described by Weibull statistics based on the weakest-link hypothesis.[35,36] The tensile strength distribution and Weibulls modulus of the as-fabricated and the heat-treated $(Y_2O_3)ZrO_2/Al_2O_3$ eutectic fibers are shown in Fig. 6. The Weibulls modulus of the $(Y_2O_3)ZrO_2/Al_2O_3$ eutectic fiber remained similar after extended thermal exposure. The Weibulls modulus (m) were measured to be 15.5 in the as-fabricated state and 15 after heat treatment at 1300°C for 300 h and 1500°C for 100 h, respectively. The results clearly demonstrate that the $(Y_2O_3)ZrO_2/Al_2O_3$ eutectic fiber grown by the EFG technique exhibits excellent strength retention after annealing at elevated temperatures in oxidizing environment.

3.2. Fracture Toughness and Crack Growth Behavior

The typical fracture morphology of the $(Y_2O_3)ZrO_2/Al_2O_3$ eutectic fibers in the as-fabricated state and after annealing at 1500°C/100 h are shown in Fig. 7(a) and (b), respectively. All the fibers exhibited brittle fracture morphology. A close examination also revealed that fracture was initiated primarily from the porosity located at the colony boundary

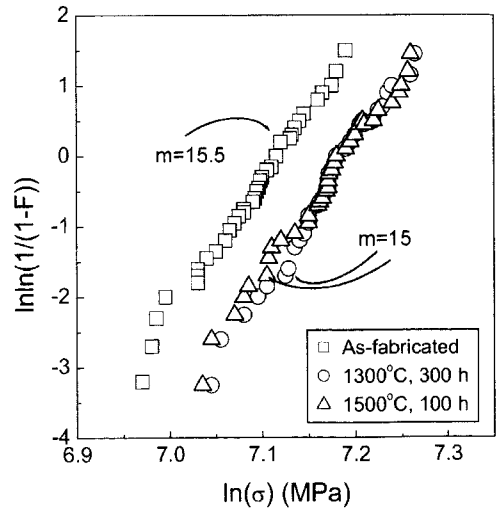

Fig. 6. Tensile strength distribution and Weibull's modulus of the $(Y_2O_3)ZrO_2/Al_2O_3$ eutectic fibers.

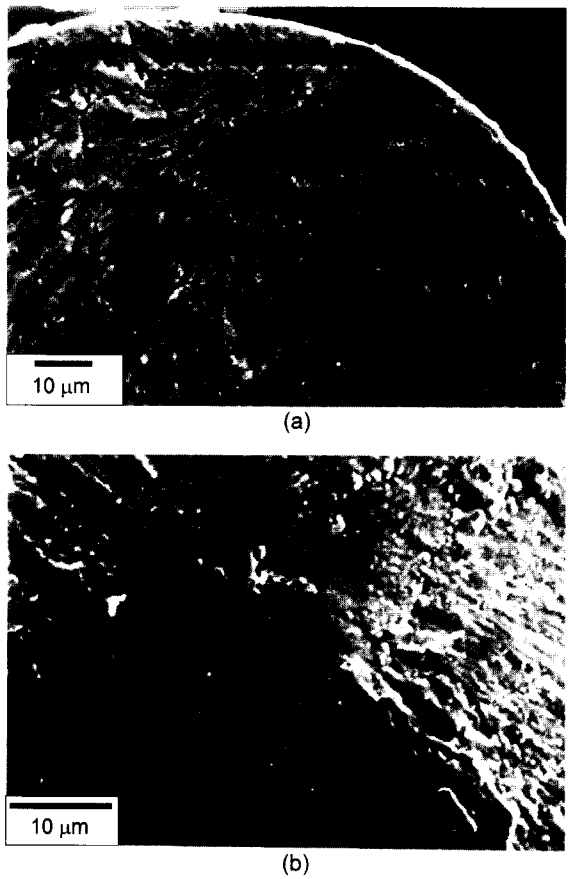

Fig. 7. The fracture morphology of $(Y_2O_3)ZrO_2/Al_2O_3$ eutectic fiber (a) as-fabricated state and (b) heat-treated at 1500°C for 100 h.

inside the fiber. None of the fiber fracture was initiated from the surface flaws or defects, which are the primary fracture initiation site for the $Y_3Al_5O_{12}/Al_2O_3$ eutectic fiber.[9] Table 1 shows the measured fracture toughness calculated by the equation (1) and (2). The average fiber strength and flaw sizes of the fiber in the as-fabricated state and after extended thermal exposure are also listed in Table 1. The average fracture toughness of the eutectic fibers calculated by the equation (1) in as-fabricated state, after heat treatment at 1300°C and 1500°C for 100 h were measured to be 2.2 ± 0.2, 2.1 ± 0.2, and 1.8 ± 0.3 MPa · $m^{1/2}$, respectively. The fracture toughness values by the equation (1) are closely related to the size of the porosity of the fiber because the flaw sizes observed in the fibers after tensile test were used in the equation (1). This means that the tensile strength of the fiber significantly depends on the size of porosity formed during the fabrication process.

Due to the limitation of the above method, other attempt was made to calculate the fracture toughness of the eutectic fiber using an indentation technique (by the equation (2)). The measured fracture toughness (K_{IC}) of the $(Y_2O_3)ZrO_2/Al_2O_3$ eutectic fiber by the indentation technique is also shown in Table 1. The average fracture toughness (K_{IC}) of the $(Y_2O_3)ZrO_2/Al_2O_3$ eutectic fiber were measured to be 3.6 ± 0.5 MPa · $m^{1/2}$, using the indentation technique. The fracture toughness measured by the equation (2) exhibits higher value than that measured by the equation (1). This discrepancy may be attributed to that the fracture toughness calculated by the equation (1) is highly dependent on the defects (porosity) formed during fabrication process of the fiber. The value, 3.6 ± 0.5 MPa · $m^{1/2}$, of the $(Y_2O_3)ZrO_2/Al_2O_3$ eutectic fiber calculated by eq. (2) is in the range between those of $Y_3Al_5O_{12}/Al_2O_3$ fiber (5.4 ± 1.7 MPa · $m^{1/2}$, ⊥ to fiber axis), CeO_2-doped $Y_3Al_5O_{12}/Al_2O_3$ composite (5.0 ± 1.5 MPa · $m^{1/2}$), and $Y_3Al_5O_{12}/Al_2O_3$ fiber (3.0 ± 0.8 MPa · $m^{1/2}$, // to fiber axis and 2.9 ± 0.3 MPa · $m^{1/2}$, 45° rotated to fiber axis), Pr_2O_3-doped $Y_3Al_5O_{12}/Al_2O_3$ composite (2.8 ± 0.2 MPa · $m^{1/2}$) as shown in Table 2. However, the $(Y_2O_3)ZrO_2/Al_2O_3$ eutectic fiber exhibits higher fracture toughness (K_{IC}) than those of MgO-doped (250 ppm) $Y_3Al_5O_{12}$ (1.9 MPa · $m^{1/2}$) and SiO_2-doped (500 ppm) $Y_3Al_5O_{12}$ (1.8 MPa · $m^{1/2}$) ceramics, using the three point bend test.[37] De With *et al.* reported the fracture toughness value of 3.7 MPa · $m^{1/2}$ for MgO-doped (5 ppm) Al_2O_3, using the three point bend test.[38]

Table 1. Measurements of Fracture Toughness (K_{IC}) of (Y_2O_3) ZrO_2/Al_2O_3 Eutectic Fiber Using Eq. (1) and Eq. (2)

	K_{IC} calculated by Eq. (1)				K_{IC} calculated by Eq. (2)
	σ (MPa)	a (μm)	c (μm)	K_{IC} (MPa·$m^{1/2}$)	K_{IC} (MPa·$m^{1/2}$)
As-fabricated	1200 ± 73	2.4 ± 0.1	2.6 ± 0.2	2.2 ± 0.2	3.6 ± 0.5
1300°C/100 h	1380 ± 102	1.1 ± 0.1	3.0 ± 0.2	2.1 ± 0.2	–
1500°C/100 h	1285 ± 110	1.0 ± 0.2	2.4 ± 0.2	1.8 ± 0.3	–

Table 2. Comparison of Measured Mechanical Properties of $(Y_2O_3)ZrO_2/Al_2O_3$, $Y_3Al_5O_{12}/Al_2O_3$ Fibers, CeO_2- and Pr_2O_3-doped $Y_3Al_5O_{12}/Al_2O_3$

Fiber	H_V (GPa)	n	K_{IC} (MPa·$m^{1/2}$)
$(Y_2O_3)ZrO_2/Al_2O_3$	18.1 ± 0.9	1.53	3.6±0.4
$Y_3Al_5O_{12}/Al_2O_3$[9]	20.4 ± 1.2	1.63	3.0 ± 0.8 (∥ to fiber axis) 5.4 ± 1.7 (⊥ to fiber axis) 2.9 ± 0.3 (45° rotated to fiber axis)
CeO_2-doped $Y_3Al_5O_{12}/Al_2O_3$[10]	34.7 ± 4.9	1.51	5.0 ± 1.5
Pr_2O_3-doped $Y_3Al_5O_{12}/Al_2O_3$[10]	16.9 ± 1.4	1.54	2.8 ± 0.2

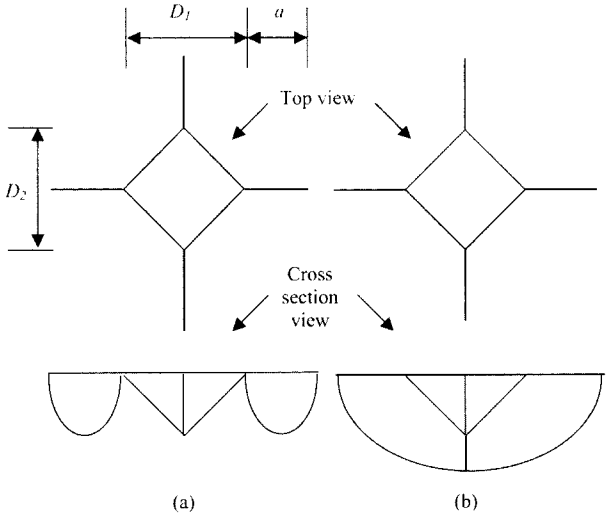

Fig. 8. Comparison of geometry between a radial (Palmqvist) and a radial-median (half-penny) cracks at Vickers indentation (a) Palmqvist cracks and (b) half-penny cracks.

Cracks produced by sharp indenter (diamond Vickers indenter) can be classified into two different types of crack morphology as shown in Fig. 8: a radial (Palmqvist) crack and a radial-median (half-penny) crack types.[39] Cracks at the 4 corners of indentation mark are four independent surface cracks referred to as Palmqvist cracks.[40] The cracks produced by Vickers diamond indenter in the $(Y_2O_3)ZrO_2/Al_2O_3$ eutectic fiber in this study was assessed using stepwise polishing as shown in Fig. 9. Fig. 9(a) and (b) show the original Vickers indentation mark on the polished surface of the $(Y_2O_3)ZrO_2/Al_2O_3$ eutectic fiber. Fig. 9(c) shows the cracking pattern at 12 μm beneath the original polished surface. Two cracks never interconnect with each other. It is evident that the $(Y_2O_3)ZrO_2/Al_2O_3$ eutectic fiber exhibits the radial (Palmqvist) crack type under the applied load of 100 g. Also, the cracks in the $(Y_2O_3)ZrO_2/Al_2O_3$ eutectic fiber propagated into all directions and exhibited an orthotropic crack propagation behavior as shown in Fig. 9(a) and (b). The cracks cut through the elongated colony and fine lamellar microstructure without being deflected along the ZrO_2/Al_2O_3 interfaces. This suggests that the bonding between ZrO_2 and Al_2O_3 phases is strong. Echigoya et al. reported an anisotropic crack growth behavior in a directionally solidified Al_2O_3-$ZrO_2(Y_2O_3)$ eutectic composite grown by a xenon lamp infrared heating furnace.[41] Microstructures of the Al_2O_3-$ZrO_2(Y_2O_3)$ eutectic in the paper reported by Echigoya *et al.*[41] did not exhibit the formation of cells and colony structure. It is believed that the different crack propagation behavior may result from the differences in microstructures. However, the anisotropic nature of crack propagation in the directionally solidified eutectic fibers is still unknown. Hardness of the $(Y_2O_3)ZrO_2/Al_2O_3$ eutectic fiber in this study was measured to be 18.1 GPa (at 1 N load) as shown in Table 2. This value is somewhat lower than those of Al_2O_3 (about 20 GPa at 1 N load),[42] $Y_3Al_5O_{12}$ (20.2 GPa at 1 N load),[37] and $Y_3Al_5O_{12}/Al_2O_3$ eutectic fiber (20.4 GPa at 1 N load).[9]

The load dependence of indentation diagonal is often described by the so-called Meyer law[37]

$$P = C \cdot D^n \tag{4}$$

where P is the indentation load, D is the arithmetic mean of the two diagonals, D_1 and D_2 as defined in Fig. 8, C is the load to make an unit size indentation, and n is a measure for the load dependence of the hardness and thus of the size effect. A typical Meyer's plot of the $(Y_2O_3)ZrO_2/Al_2O_3$ eutectic fibers is shown in Fig. 10. The measured n was 1.53 from the Meyers plot, using a weighted least-squares analysis of indentation diagonal length versus load. This n value (1.53) is typical in ceramics[37] and is similar to the $Y_3Al_5O_{12}/Al_2O_3$ eutectic fiber.[9] The change of Palmqvist crack length, a, according to the suggested equation,[32] $a = (P - P_0)/4W$ (where P_0 is a threshold indentation load for crack initiation), plotted as a function of indentation load in the $(Y_2O_3)ZrO_2/Al_2O_3$ eutectic fiber is shown in Fig. 11. It is clear that there exists a linear relationship between the Palmqvist crack length and the indentation load. The $Y_3Al_5O_{12}/Al_2O_3$ eutectic fiber exhibited the same linear behavior.[9] Shetty *et al.* reported similar linear relationship between Palmqvist crack length and the indentation load in glass-ceramic (Pyro-

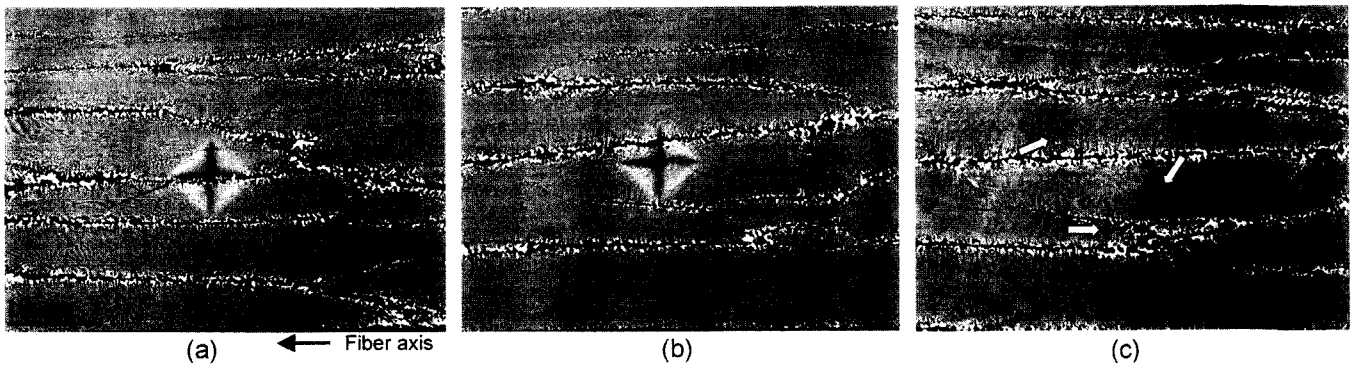

Fig. 9. Cracking patterns of the $(Y_2O_3)ZrO_2/Al_2O_3$ fiber under indentation load of 100 g (a) and (b) in the as-fabricated states, and (c) Vickers indentation mark showing Palmqvist crack type after 12 μm removed from the original polished surface of Fig. 5(b).

ceram 9606, Corning Glass Works, Corning, NY).[32] Also, the linear change was found in WC-Co cemented carbides.[40]

4. Conclusion

The microstructure of the directionally solidified $(Y_2O_3)ZrO_2/Al_2O_3$ eutectic fiber grown by EFG technique consists of highly oriented colony and fine lamellar microstructure within the colony. After extended heat treatment, the coarsening of the fine lamellar structure was observed. The main driving force is to reduce the interfacial energy in the eutectic structure through interface and volume diffusion process. The kinetics of lamellar coarsening and morphology rearrangement during coarsening is discussed elsewhere.[8] The room-temperature tensile strength of the $(Y_2O_3)ZrO_2/Al_2O_3$ eutectic fiber (1.2 GPa) is lower than that of the c-axis Al_2O_3 fiber (> 3 GPa) and $Y_3Al_5O_{12}/Al_2O_3$ eutectic fiber (~2 GPa).[15] This may be due to the presence of processing defects at the eutectic colony boundaries, which serve as the primary flaw for fracture initiation. However, the $(Y_2O_3)ZrO_2/Al_2O_3$ eutectic fibers grown by the EFG technique exhibit excellent strength retention after heat treatment at temperature up to 1500°C. The excellent strength retention after annealing may be attributed to a compressive stress in the ZrO_2 matrix resulting from the increase in volume during the cubic-to-monoclinic transformation.

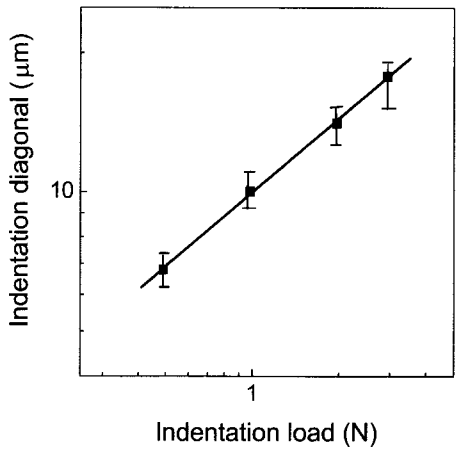

Fig. 10. The changes of indentation diagonal as a function of indentation load for the $(Y_2O_3)ZrO_2/Al_2O_3$ eutectic fiber in the as-fabricated state.

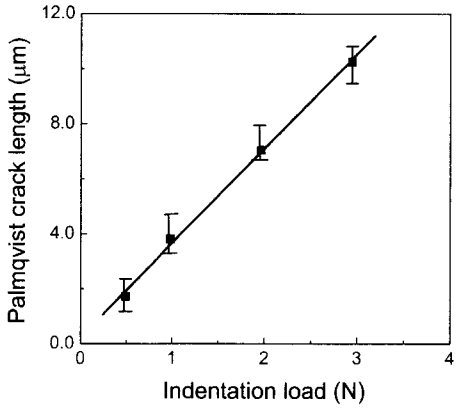

Fig. 11. Load dependence of Palmqvist crack length for the $(Y_2O_3)ZrO_2/Al_2O_3$ eutectic fiber in the as-fabricated state.

The $(Y_2O_3)ZrO_2/Al_2O_3$ eutectic fiber exhibited the radial (Palmqvist) crack type and orthotropic crack propagation behavior under 100 g load. Fracture toughness of the as-fabricated fiber was measured to be 2.2 ± 0.2 $MPam^{1/2}$ by assuming elliptical flaw of a semi-infinite solid and 3.6 ± 0.5 $MPam^{1/2}$ using an indentation technique, respectively. The measured hardness value of the $(Y_2O_3)ZrO_2/Al_2O_3$ eutectic fiber, 18.1 GPa, was lower than those of Al_2O_3, $Y_3Al_5O_{12}$, and $Y_3Al_5O_{12}/Al_2O_3$ eutectic fiber. The $(Y_2O_3)ZrO_2/Al_2O_3$ eutectic fiber exhibits a linear behavior of indentation diagonal with indentation load. Also, there exists a linear relationship between Palmqvist crack length and indentation load.

Acknowledgement

The results shown in Figs. 4, 6, and 7 are based on experiments performed by Dr. X. Q. Zhu.

REFERENCES

1. S. A. Newcomb and R. E. Tressler, "Slow Crack Growth in Sapphire Fibers at 800° to 1500°C," *J. Am. Cerem. Soc.*, **76** [10] 2505-12 (1993).
2. J. E. Sheehan, J. Sigalovsky, J. S. Haggerty, and J. R. Porter, "Mechanical Properties of $MgAl_2O_4$ Single Crystal Fibers," *Ceram. Eng. Sci. Proc.*, **14** [7-8] 660-70 (1993).
3. K. J. McClellan, H. Sayir, A. H. Heuer, A. Sayir, J. Haggerty, and J. Sigalovsky, "High-strength, Creep-resistant Y_2O_3-stabilized Cubic-ZrO_2 Single Crystal Fibers," *Ceram. Eng. Sci. Proc.*, **14** [7-8] 651-59 (1993).
4. G. S. Corman, "Strength and Creep of Single Crystal YAG Fibers," Presented at the 94th Annual Meeting of the American Ceramic Society, Minneapolis, MN, April 12-16 (1992).
5. S. Kim, S. Kim, and W. C. LaCourse, "ZrO_2 Ceramic Fiber Fabrication by Sol-gel Processing," *J. Kor. Ceram. Soc.*, **27** [6] 824-28 (1990).
6. I.-H. Song, S.-U. Kim, and M.-S. Yoon, "Fabrication of Zirconia Ceramic Fiber by Sol-gel Processing: (II) The Doping Effect of CaO on their Microstructure and Phase Transition," *J. Kor. Ceram. Soc.*, **28** [10] 819-23 (1991).
7. C. Whang, H. Eun, and H. Kwon, "Fabrication of Y_2O_3-ZrO_2 and CaO-ZrO_2 Fibers by Sol-gel Process and their Phase Characterization by Raman Microprobe," *J. Kor. Ceram. Soc.*, **31** [1] 104-14 (1994).
8. D.-Y. Park, J.-M. Yang, and J. M. Collins, "Coarsening of Lamella Microstructures in Directionally Solidified Yttrium Aluminate/Alumina Eutectic Fiber," *J. Am. Ceram. Soc.*, **84** [12] 2991-96 (2001).
9. D.-Y. Park and J.-M. Yang, "Effect of the Microstructure on the Mechanical Properties of a Directionally Solidified $Y_3Al_5O_{12}/Al_2O_3$ Eutectic Fiber," *J. Mater. Sci.*, **36** 5593-601 (2001).
10. D.-Y. Park and J.-M. Yang, "Fracture Behavior of Direction-

ally Solidified CeO_2- and Pr_2O_3-doped $Y_3Al_5O_{12}/Al_2O_3$ Eutectic Composites," *Mater. Sci. Eng.*, **A332** 276-84 (2002).
11. S. C. Farmer, A. Sayir, and P. O. Dickerson, "Mechanical and Microstructural Characterization of Directionally Solidified Alumina-Zirconia Eutectic Fibers," *in In Situ Composites: Science and Technology*. The Metallurgical Society, Warrendale, PA, p.167 (1993).
12. E. L. Courtright, J. S. Haggerty, and J. Sigalovsky, "Controlling Microstructures in $ZrO_2(Y_2O_3)$-Al_2O_3 Eutectic Fibers," *Ceram. Eng. Sci. Proc.*, **14** [7-8] 671-81 (1993).
13. H. E. Bates, "EFG Growth of Alumina-Zirconia Eutectic Fiber," *Ceram. Eng. Sci. Proc.*, **13** [7-8] 190-97 (1992).
14. T. Mah, T. A. Parthasarathy, M. D. Petry, and L. E. Matson, "Processing, Microstructure, and Properties of Al_2O_3-$Y_3Al_5O_{12}$ (YAG) Eutectic Fibers," *Ceram. Eng. Sci. Proc.*, **14** [7-8] 622-38 (1993).
15. J.-M. Yang, S. M. Jeng, and S. K. Chang, "Fracture Behavior of Directionally Solidified $Y_3Al_5O_{12}/Al_2O_3$ Eutectic Fiber," *J. Am .Ceram. Soc.*, **79** [5] 1218-22 (1996).
16. S. C. Famer, A. Sayir, P. O. Dickerson, and S. L. Draper, "Microstructural Stability and Strength Retention in Directionally Solidified Al_2O_3-YAG Eutectic Fibers," *Ceram. Eng. Sci. Proc.*, **16** [5] 969-76 (1995).
17. G. R. Fischer, L. J. Manfredo, R. N. McNally, and R. C. Doman, "The Eutectic and Liquidus in the Al_2O_3-ZrO_2 System," *J. Mater. Sci.*, **16** 3447-51 (1981).
18. W. D. Tuohig and T. Y. Tien, *J. Am. Ceram. Soc.*, **63** [9-10] 595-96 (1980).
19. C. O. Hulse and J. A. Batt, ONR Report AD-781955 (1974).
20. J. Echigoya, Y. Takabayashi, H. Suto, and M. Ishigame, "Structure and Crystallography of Directionally Solidified Al_2O_3-ZrO_2-Y_2O_3 Eutectic by the Floating Zone Melting Method," *J. Mater. Sci. Lett.*, **5** 150-52 (1986).
21. A. G. Evans and E. A. Charles, "Fracture Toughness Determinations by Indentation," *J. Am. Ceram. Soc.-Discussion and Notes*, **59** [7-8] 371-72 (1976).
22. B. R. Lawn and E. R. Fuller, "Equilibrium Penny-like Cracks in Indentation Fracture," *J. Mater. Sci.*, **10** 2016-24 (1975).
23. A. G. Evans, in: R. C. Bradt, D. H. P. Hasselman, and F. F. Lange (Ed.), "Fracture Mechanics of Ceramics," Plenum Press, NY, p. 17 (1974).
24. J.-M. Yang and X. Q. Zhu, "Thermo-mechanical Stability of Directionally Solidified Al_2O_3-$ZrO_2(Y_2O_3)$ Eutectic Fibers," *Script. Mater.*, **36** [9] 961-66 (1997).
25. R. W. Hertzberg (Ed.), Deformation and Fracture Mechanics of Engineering Materials, the 4th Ed. John Wiley & Sons Inc., p. 347 (1996).
26. A. G. Evans and T. R. Wilshaw, "Quasi-static Solid Particle Damage in Brittle Solids-I. Observations, Analysis and Implications," *Acta Metall.*, **24** 939-56 (1976).
27. B. Lawn and R. Wilshaw, "Indentation Fracture : Priciples and Applications," *J. Mater. Sci.*, **10** 1049-81 (1975).
28. B. Lawn, "Fracture of Brittle Solids," Cambridge University Press, Cambridge, U.K., Chap. 8 (1993).
29. D. Tabor, "Hardness of Metals," Clarendon, Oxford, U.K. (1951).
30. H. E. LaBelle, Jr. and A. I. Mlavsky, "Growth of Controlled Profile Crystals from the Melt : Part I Sapphire Filaments," *Mat. Res. Bull.*, **6** 571-80 (1971).
31. H. E. LaBelle, Jr., "EFG, the Invention and Application to Sapphire Growth," *J. Cryst. Growth*, **50** 8-17 (1980).
32. D. K. Shetty, A. R. Rosenfield, and W. H. Duckworth, "Indenter Flaw Geometry and Fracture Toughness Estimates for a Glass-ceramic," *J. Am. Ceram. Soc.*, 68 [10] C-282-C-284 (1985).
33. A. Sayir, in: A. Pechenik, R. K. Kalia, and P. Vashishta (Ed.), "Directional Solidification of Eutectic Ceramics," in Computer-aided Design of High-temperature Materials, Oxford University Press, Oxford, U.K. (1999).
34. F. L. Kennard, R. C. Bradt, and V. S. Stubican, "Directional Solidification of the ZrO_2-MgO Eutectic," *J. Am. Ceram. Soc.*, **57** [10] 428-31 (1974).
35. W. Weibull and R. Swed, *Acad. Eng. Sci. Pro.*, **151** 1 (1939).
36. K. Trustrum and A. De S. Jayatilaka, "On Estimating the Weibull Modulus for a Brittle Material," *J. Mater. Sci.*, **14**, 1080-84 (1979).
37. G. de With and J. E. D. Parren, "Translucent $Y_3Al_5O_{12}$ Ceramics : Mechanical Properties," *Solid State Ionics*, **16** 87-94 (1985).
38. G. de With, "Fracture of Translucent Alumina: Temperature Dependence and Influence of CaO Dope," *J. Mater. Sci.*, **19** 2195-202 (1984).
39. D. K. Shetty, I. G. Wright, P. N. Mincer, and A. H. Clauer, "Indentation Fracture of WC-Co Cermets," *J. Mater. Sci.*, **20** 1873-82 (1985).
40. H. E. Exner, "The Influence of Sample Preparation on Palmqvists Method for Toughness Testing of Cemented Carbides," *Trans. Met. Soc. AIME*, **245** 677-83 (1969).
41. J. Echigoya, Y. Takabayashi, and H. Suto, "Hardness and Fracture Toughness of Directionally Solidified Al_2O_3-$ZrO_2(Y_2O_3)$ Eutectics," *J. Mater. Sci. Lett.*, **5** 153-54 (1986).
42. D. J. Clinton and R. Morrell, "The Hardness of Alumina Ceramics," *Brit. Ceram. Proc.*, **34** 113-27 (1984).
43. R. K. Viswanadham and J. D. Venables, "A Simple Method for Evaluating Cemented Carbides," *Metall. Trans. A*, **8A** 187-91 (1977).